

## Trinuclear metal clusters in catalysis by terpenoid synthases\*

Julie A. Aaron and David W. Christianson<sup>‡</sup>

*Roy and Diana Vagelos Laboratories, Department of Chemistry, University of Pennsylvania, Philadelphia, PA 19104-6323, USA*

**Abstract:** Terpenoid synthases are ubiquitous enzymes that catalyze the formation of structurally and stereochemically diverse isoprenoid natural products. Many isoprenoid coupling enzymes and terpenoid cyclases from bacteria, fungi, protists, plants, and animals share the class I terpenoid synthase fold. Despite generally low amino acid sequence identity among these examples, class I terpenoid synthases contain conserved metal-binding motifs that coordinate to a trinuclear metal cluster. This cluster not only serves to bind and orient the flexible isoprenoid substrate in the precatalytic Michaelis complex, but it also triggers the departure of the diphosphate leaving group to generate a carbocation that initiates catalysis. Additional conserved hydrogen bond donors assist the metal cluster in this function. Crystal structure analysis reveals that the constellation of three metal ions required for terpenoid synthase catalysis is generally identical among all class I terpenoid synthases of known structure.

**Keywords:** enzyme catalysis; farnesyl diphosphate; geranyl diphosphate; inorganic pyrophosphate; Mg<sup>2+</sup>.

### INTRODUCTION

The terpenome is comprised of a family of more than 55 000 structurally and stereochemically diverse natural products, all of which ultimately derive from the universal 5-carbon precursors dimethylallyl diphosphate (DMAPP) and isopentenyl diphosphate (IPP) (Fig. 1) [1]. Terpenoids are ubiquitous throughout nature and serve a multitude of specific functions in plants, animals, insects, bacteria, and fungi. For example, terpenoids are critical for plant survival and account for a large number of primary metabolites, including molecules involved in photosynthesis, respiration, and membrane structure. Terpenoids also account for a wide range of secondary metabolites in plants, where they bestow unique flavors and fragrances, provide chemical defense against pests, and facilitate interactions between plants and other organisms [2,3]. From a medicinal perspective, terpenoids are of great interest because many of these natural products exhibit anti-cancer, -malarial, and -microbial activities [2]. In humans, the 15-carbon linear isoprenoid farnesyl diphosphate (FPP) is a precursor in the biosynthesis of steroids and is also utilized for posttranslational prenylation of Ras in GTPase signaling [4,5]. Recently, human FPP synthase has been identified as the target of nitrogen-containing bisphosphonate drugs used for the treatment of bone diseases such as osteoporosis, hypercalcemia, and metastatic bone disease [6,7].

---

\*Paper based on a presentation on the “Chemistry for Health” theme at the 42<sup>nd</sup> IUPAC Congress, 2–7 August 2009, Glasgow, UK. Other Congress presentations are published in this issue, pp. 1569–1717.

<sup>‡</sup>Corresponding author

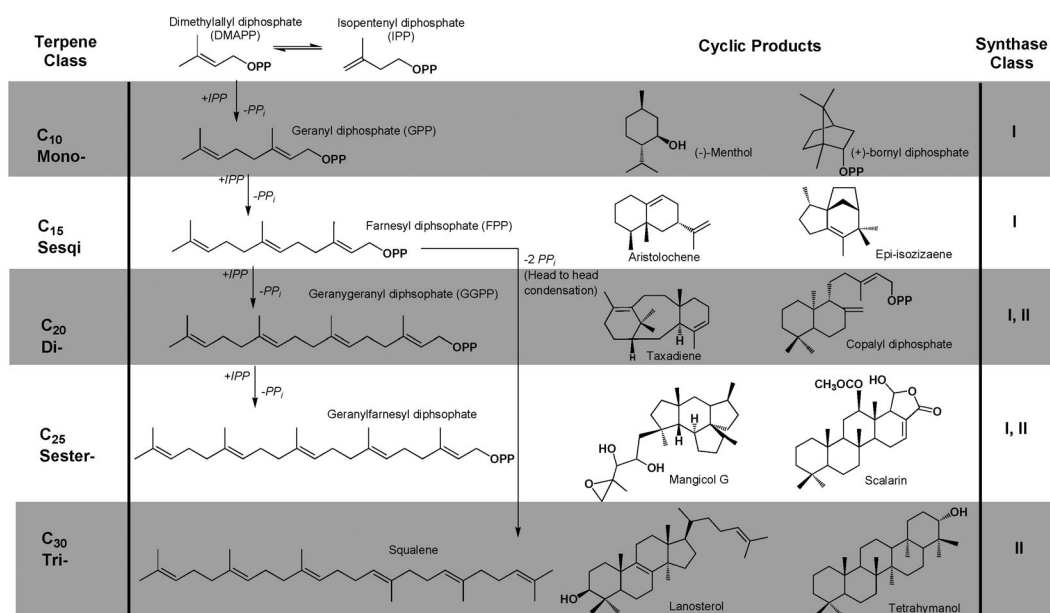


**Fig. 1** General scheme of terpenoid nomenclature and biosynthesis (OPP = diphosphate,  $PP_i$  = inorganic diphosphate).

Terpenoid synthases can be divided into two categories: class I enzymes adopt the FPP synthase  $\alpha$ -helical fold and initiate catalysis by metal-triggered ionization of the substrate diphosphate group, and class II enzymes adopt an unrelated double  $\alpha$ -barrel fold and initiate catalysis by protonation of an epoxide ring or carbon–carbon double bond (Fig. 2). Class I terpenoid synthases can be further subdivided into three categories: coupling enzymes that catalyze chain elongation reactions to form increasingly longer polyisoprenoid diphosphates, coupling enzymes that catalyze irregular (i.e., non-head-to-tail) isoprenoid condensation reactions such as cyclopropanation, cyclobutane, or branching reactions [8], and cyclization enzymes that catalyze the conversion of linear isoprenoid substrates into single and multi-ringed hydrocarbon products [9–12]. The potential diversity of carbon–carbon bond formation afforded by the flexible linear isoprenoid substrate, and the chemical potential for subsequent

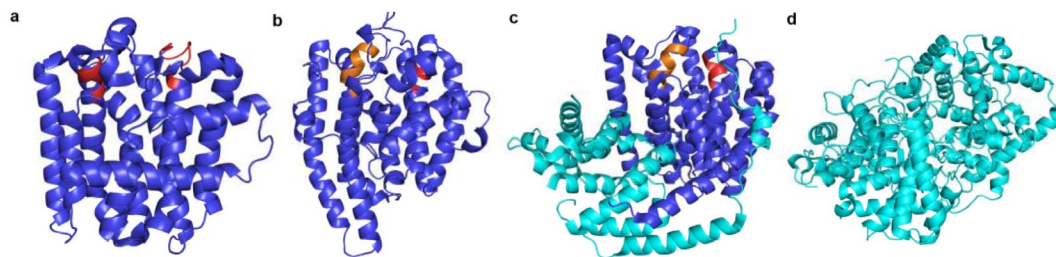


**Fig. 2** Structural similarities among various terpenoid synthases define the core class I terpenoid cyclase fold (blue). Conserved metal-binding motifs are the aspartate-rich motifs (red) and “NSE/DTE” motifs (orange) highlighted in (a) *E. coli* FPP synthase (PDB code 1RQI), (b) epi-isozizaene synthase (PDB code 3KB9), and (c) (+)-bornyl diphosphate synthase (PDB code 1N22), which contains an additional N-terminal domain (cyan). This  $\alpha$ -helical domain is topologically similar to the  $\alpha$ -barrel fold of the class II terpenoid cyclases, which occurs in a double domain architecture in the triterpene cyclase (d) oxidosqualene cyclase (PDB code 1W6K).

biosynthetic functionalization of cyclic terpenoids by cytochromes P450, monooxygenases, etc., make terpenoid biosynthesis an attractive system for engineering novel compounds [2,13,14]

To date, the crystal structures of several class I terpenoid coupling and cyclization enzymes have been solved, revealing a conserved  $\alpha$ -helical terpenoid synthase fold across all domains of life. Structures of enzyme complexes with substrates, inhibitors, and/or products have also revealed the universal conservation of a trinuclear metal cluster implicated in the molecular recognition of the substrate diphosphate group as well as the initiation of catalysis. Metal ions are coordinated by metal-binding motifs on opposing helices near the mouth of the active site. The metal-binding motifs are generally described as either “aspartate-rich” [DDXX(XX)D/E] or “NSE/DTE” [(N,D)D(L,I,V)X(S,T)XXXE], in which boldface residues typically coordinate to catalytically obligatory  $Mg^{2+}$  or  $Mn^{2+}$  ions (throughout this review, metal ligands are indicated in boldface) [15]. X-ray crystal structures have been instrumental in understanding the catalytic mechanisms of terpenoid synthases: the active site of each synthase provides a template that binds the flexible substrate(s) in the proper orientation and conformation so that, upon the departure of the diphosphate leaving group and resultant generation of a reactive carbocation, the active site template ensures a specific trajectory of inter- and intramolecular carbon-carbon bond formation in the ensuing cyclization cascade [16]. Here, we review the available crystal structures of class I terpenoid synthases complexed with trinuclear metal clusters and isoprenoid diphosphates or inorganic pyrophosphate ( $PP_i$ ) to highlight conserved structural aspects of 3-metal ion catalysis in terpenoid biosynthesis.

## ISOPRENOID COUPLING ENZYMES

### FPP synthase

FPP synthase, the archetypical prenyltransferase, catalyzes the formation of FPP, the linear isoprenoid precursor of sesquiterpene natural products. Chain elongation to form FPP proceeds in two distinct steps (Fig. 1): first, IPP and DMAPP are coupled to form GPP, and then a second molecule of IPP is coupled to GPP to form FPP. The first crystal structure of FPP synthase was that of the avian enzyme [17], which revealed a novel  $\alpha$ -helical fold. The structure revealed two conserved aspartate-rich (DDXXD) sequences [18] on helices D and H, which flank the mouth of the active site cavity. Additionally, a single  $Sm^{3+}$  ion, used for heavy metal derivatization for MIR phasing, was bound by each DDXXD motif.

The crystal structure of *E. coli* FPP synthase was the first to reveal the binding of a trinuclear magnesium cluster in the active site of an isoprenoid coupling enzyme [19], similar to the trinuclear magnesium clusters previously observed in fungal and plant terpenoid cyclases [20,21]. The structure of *E. coli* FPP synthase was solved as the enzyme-substrate ternary complex with the noncleavable DMAPP analog, dimethylallyl *S*-thiolodiphosphate (DMSPP), and a molecule of IPP. Applying the  $Mg^{2+}_A$ ,  $Mg^{2+}_B$ , and  $Mg^{2+}_C$  nomenclature first established for the trinuclear magnesium cluster of trichodiene synthase [20], the crystal structure of the *E. coli* FPP synthase- $Mg^{2+}_3$ -DMSPP-IPP complex reveals octahedral coordination of all three metal ions (Fig. 3a):  $Mg^{2+}_A$  is coordinated by D105 and D111 of the first aspartate-rich motif on helix D, two diphosphate oxygen atoms, and two water molecules;  $Mg^{2+}_C$  is coordinated by the side chains of D105, and D111, as well as one diphosphate oxygen and three water molecules; and  $Mg^{2+}_B$  is coordinated by D244 of the second aspartate-rich motif, two diphosphate oxygen atoms, and three water molecules. The diphosphate group of DMSPP also accepts hydrogen bonds from R116, K202, and K258.

More recently, the structure of the human FPP synthase- $Mg^{2+}_3$ -zoledronate-IPP complex [4] reveals complete conservation of  $Mg^{2+}_3$ -diphosphate recognition between *E. coli* and human FPP synthases (Fig. 3b). In human FPP synthase, two DDXXD motifs coordinate to the  $Mg^{2+}_3$  cluster: the first aspartate of the **D**<sup>103</sup>DDXXD<sup>107</sup> motif coordinates to  $Mg^{2+}_A$  and  $Mg^{2+}_C$  with *syn,syn*-bidentate geometry, and one oxygen atom of D107 bridges  $Mg^{2+}_A$  and  $Mg^{2+}_C$  with *syn,anti*-coordination stereochem-

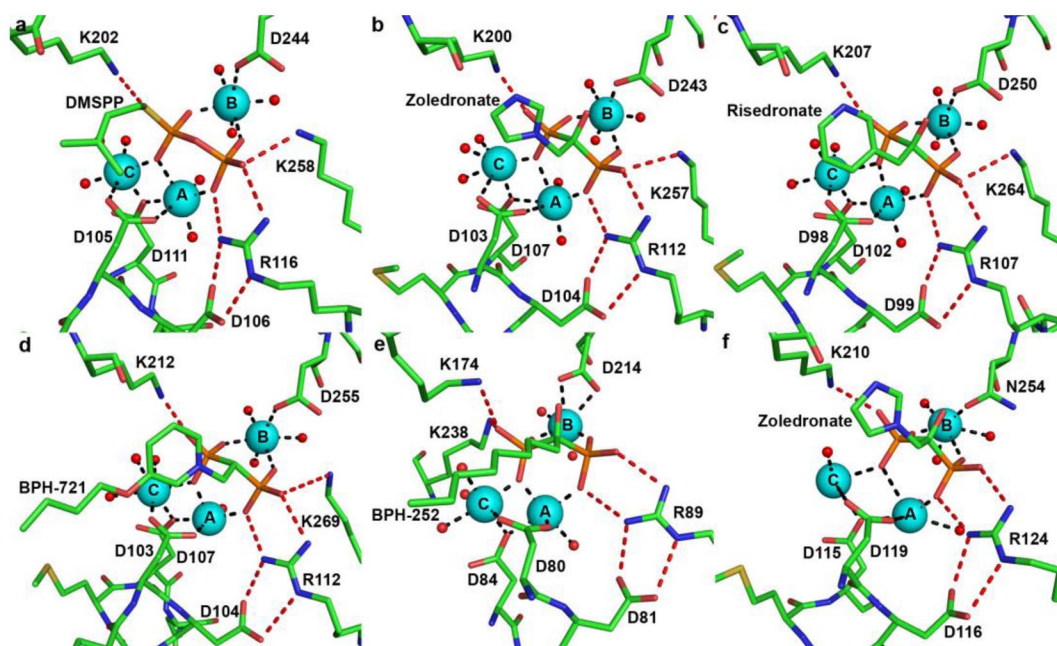


**Fig. 3** Conservation of  $\text{Mg}^{2+}_3\text{-PP}_i$  and -diphosphate binding motifs among isoprenoid coupling enzymes. Metal coordination (black) and hydrogen bond (red) interactions with phosphate(s) are indicated. (a) *E. coli* FPP synthase- $\text{Mg}^{2+}_3$ -DMSPP-IPP complex (PDB code 2EGW); (b) human FPP synthase- $\text{Mg}^{2+}_3$ -zoledronate complex (PDB 2F8Z); (c) *T. cruzi* FPP synthase- $\text{Mg}^{2+}_3$ -risedronate complex (PDB code 1YHL); (d) *T. brucei* FPP synthase- $\text{Mg}^{2+}_3$ -BPH-721 complex (PDB code 3DYH); (e) *S. cerevisiae* GGPP synthase- $\text{Mg}^{2+}_3$ -BPH-252 complex (PDB code 2Z4X); (f) *C. parvum* nonspecific prenyl synthase- $\text{Mg}^{2+}_3$ -zoledronate complex (PDB code 2Q58).

istry; the first aspartate of the second  $\text{D}^{243}\text{DXXD}$  motif coordinates to  $\text{Mg}^{2+}_B$ . The diphosphate moiety additionally accepts hydrogen bonds from R112, K200, and K257.

Interestingly, the closed active site conformation is also stabilized by newly formed hydrogen bonds between K266 and D107 and D174. The root mean square (rms) deviation between the unliganded enzyme and the closed conformation of the  $\text{Mg}^{2+}_3$ -zoledronate-IPP complex is 1.3 Å (341 C $\alpha$  atoms). Analysis of X-ray crystal structures of several human FPP synthase- $\text{Mg}^{2+}_3$ -bisphosphonate complexes suggests a two-step mechanism for substrate binding [4]. First, the binding of DMAPP and 3  $\text{Mg}^{2+}$  ions brings together the two DDXXD motifs, and loops D-E and H-I come together to form a hydrogen bond between T111 and the backbone of I258. These structural changes close the entrance to the allylic binding site and complete the formation of the IPP binding site. Secondly, as IPP binds, and as the basic C-terminal tail of the enzyme becomes ordered and closes the IPP binding site, IPP and DMAPP are properly oriented for catalysis.

The binding of a trinuclear magnesium cluster is similarly conserved in FPP synthases from parasitic organisms. The flagellated protozoan *T. cruzi* causes Chagas disease, primarily in Latin America [22]. Bisphosphonates have emerged as a potential treatment for Chagas disease by inhibiting *T. cruzi* FPP synthase [23]. The crystal structures of *T. cruzi* FPP synthase- $\text{Mg}^{2+}_3$ -inhibitor complexes [24] suggest conservation of the trinuclear magnesium cluster for substrate binding and catalysis. In the complex with risedronate (Fig. 3c), the first carboxylate of the  $\text{D}^{98}\text{DXXD}^{102}$  motif on helix D coordinates to  $\text{Mg}^{2+}_A$  and  $\text{Mg}^{2+}_C$  with *syn,syn*-bidentate geometry, and one oxygen atom of D102 bridges  $\text{Mg}^{2+}_A$  and  $\text{Mg}^{2+}_C$  with *syn,anti*-coordination stereochemistry. The first carboxylate of the  $\text{D}^{250}\text{DXXD}$  motif

on helix H is the only residue that directly coordinates to  $\text{Mg}^{2+}_{\text{B}}$ ; however, D251 and D254 indirectly interact with  $\text{Mg}^{2+}_{\text{B}}$  via bridging water molecules. Each  $\text{Mg}^{2+}$  ion is coordinated with octahedral geometry, with nonprotein coordination sites occupied by oxygen atoms of the inhibitor phosphonate groups and water molecules. Oxygen atoms of the two risedronate phosphonate groups accept hydrogen bonds from the side chains of R107, K207, and K264.

*Trypanosoma brucei* is an African parasitic protist, and its FPP synthase is related to that of *T. cruzi* by 70 % amino acid sequence identity. The crystal structure of *T. brucei* FPP synthase complexed with  $\text{Mg}^{2+}_3$ -BPH-721 [25] reveals conservation of the trinuclear magnesium cluster for substrate binding and catalysis (Fig. 3d). The first carboxylate of the **D<sup>103</sup>DXXD<sup>107</sup>** motif on helix D coordinates to  $\text{Mg}^{2+}_{\text{A}}$  and  $\text{Mg}^{2+}_{\text{C}}$  with *syn,syn*-bidentate geometry, and one oxygen atom of D107 bridges  $\text{Mg}^{2+}_{\text{A}}$  and  $\text{Mg}^{2+}_{\text{C}}$  with *syn,anti*-coordination stereochemistry. The first aspartate in the **D<sup>255</sup>DXXD** motif on helix H is the only residue that directly coordinates to  $\text{Mg}^{2+}_{\text{B}}$ ; however, D256 and D259 indirectly interact with  $\text{Mg}^{2+}_{\text{B}}$  via bridging water molecules. Oxygen atoms of the two phosphonate groups of the inhibitor BPH-721 also accept hydrogen bonds from the side chains of R112, K212, and K269 [26].

### Geranylgeranyl diphosphate synthase, nonspecific prenyl synthase

Geranylgeranyl diphosphate synthase (GGPP synthase) catalyzes the condensation of IPP and FPP to form GGPP (Fig. 1). Recently, GGPP synthase has emerged as a pharmaceutical target for the treatment of cancer since geranylgeranylation is involved in Rac, Rap, and Rho signaling pathways [27]. The crystal structures of GGPP synthases from *Thermus thermophilus* [28], *Sinapis alba* [29], and *Saccharomyces cerevisiae* [30] have been determined in addition to that of human GGPP synthase [31]. However, a crystal structure containing a complete trinuclear magnesium cluster has only been observed in the active site of monomer B of the *S. cerevisiae* GGPP synthase- $\text{Mg}^{2+}_3$ -BPH-252 complex (Fig. 3e) [32]. The first aspartate of the **D<sup>80</sup>DIED<sup>84</sup>** motif coordinates to  $\text{Mg}^{2+}_{\text{A}}$  and  $\text{Mg}^{2+}_{\text{C}}$  with *syn,syn*-bidentate geometry, and one oxygen atom of D84 bridges  $\text{Mg}^{2+}_{\text{A}}$  and  $\text{Mg}^{2+}_{\text{C}}$  with *syn,anti*-coordination stereochemistry; the first aspartate of the second **D<sup>214</sup>DYLN** motif coordinates to  $\text{Mg}^{2+}_{\text{B}}$ . Each  $\text{Mg}^{2+}$  ion is coordinated with octahedral geometry, with nonprotein coordination sites occupied by oxygen atoms of the inhibitor phosphonate groups and water molecules. Oxygen atoms of the two phosphonate groups of the inhibitor BPH-252 also accept hydrogen bonds from R89, K174, and K238.

Recently, the crystal structure of a nonspecific prenyl synthase from *Cryptosporidium parvum* has been determined [33]. *C. parvum* causes livestock infections and is classified as a bioterrorism threat by the Centers for Disease Control and Prevention [34]. The enzyme has a unique ability to catalyze chain elongation reactions with isoprenoid substrates of various lengths to generate  $\text{C}_{20}$ – $\text{C}_{45}$  linear isoprenoids products. The crystal structure of the enzyme reveals conservation of the classic  $\alpha$ -helical terpenoid synthase fold, and its complex with the inhibitor risedronate reveals that a complete trinuclear magnesium cluster is coordinated by DDXXD and NDXXD motifs (Fig. 3f) [33]. The first carboxylate of the **D<sup>115</sup>DXXD<sup>119</sup>** motif on helix D is oriented for coordination to  $\text{Mg}^{2+}_{\text{A}}$  and  $\text{Mg}^{2+}_{\text{C}}$  with *syn,syn*-bidentate geometry; however, the distance between D115 and  $\text{Mg}^{2+}_{\text{C}}$  is 3.14 Å, thus too long to be considered an inner-sphere metal coordination interaction. One oxygen atom of the third aspartate, D119, bridges  $\text{Mg}^{2+}_{\text{A}}$  and  $\text{Mg}^{2+}_{\text{C}}$  with *syn,anti*-coordination stereochemistry. N254 of the **N<sup>254</sup>DXXD** motif on helix H coordinates to  $\text{Mg}^{2+}_{\text{B}}$ , and D255 and D258 indirectly interact with  $\text{Mg}^{2+}_{\text{B}}$  via bridging waters. The diphosphate moiety additionally accepts hydrogen bonds from K210 and G251, and the closed active site conformation is stabilized by hydrogen bonds between D116 of the DDXXD motif and R124, and D255 of the NDXXD motif and Q251.

## ISOPRENOID CYCLIZATION ENZYMES

## Fungal cyclases

The sesquiterpene cyclase trichodiene synthase from *Fusarium sporotrichioides* catalyzes the first committed step in the biosynthesis of nearly 100 different trichothecene mycotoxins. Trichodiene synthase is one of the most thoroughly studied terpenoid cyclases, and enzymological and crystallographic studies have illuminated important features in the cyclization mechanism (reviewed in [15]). Recent computational studies have also provided new insight on the catalytic mechanism [35]. The structures of unliganded trichodiene synthase and the trichodiene synthase-Mg<sup>2+</sup><sub>3</sub>-PP<sub>i</sub> complex were the first to reveal the binding of a trinuclear magnesium cluster in the active site of a terpenoid synthase (Fig. 4a) [20]. The first aspartate of the D<sup>100</sup>DXXD motif on helix D coordinates to Mg<sup>2+</sup><sub>A</sub> and Mg<sup>2+</sup><sub>C</sub> with *syn,syn*-bidentate geometry. The second metal-binding motif N<sup>225</sup>DLMS<sup>229</sup>FYKE<sup>333</sup> is located on helix H and coordinates to Mg<sup>2+</sup><sub>B</sub>. All three metal ions are additionally coordinated by PP<sub>i</sub> and solvent molecules to complete octahedral coordination polyhedra.

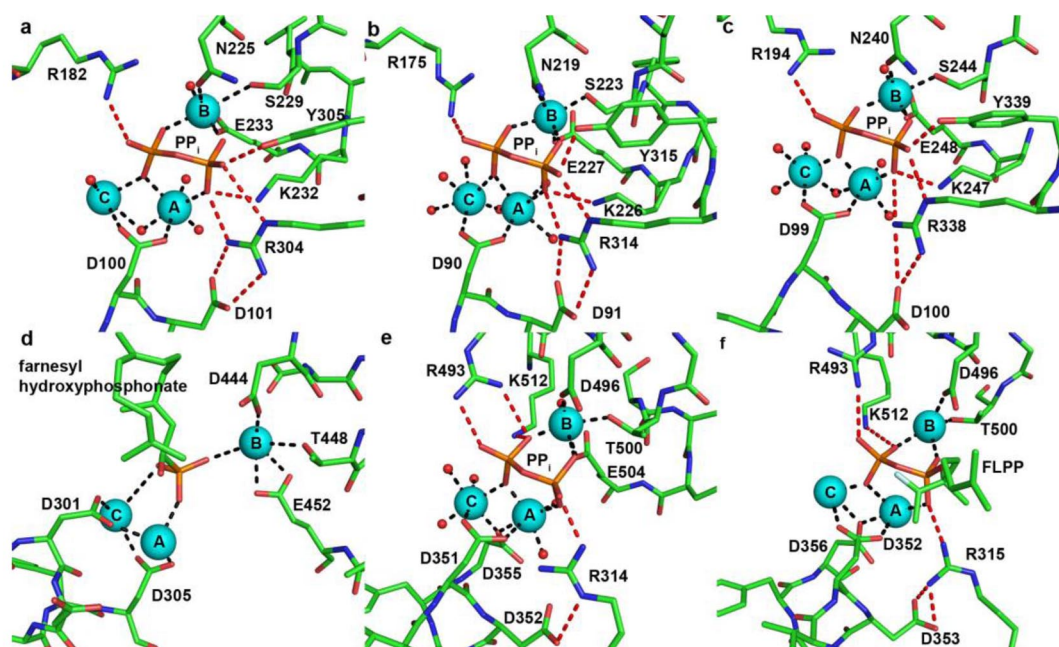


**Fig. 4** Conservation of Mg<sup>2+</sup><sub>3</sub>-PP<sub>i</sub> and -diphosphate binding motifs among terpenoid cyclases. Metal coordination (black) and hydrogen bond (red) interactions with phosphate(s) are indicated. (a) *F. sporotrichioides* trichodiene synthase-Mg<sup>2+</sup><sub>3</sub>-PP<sub>i</sub> complex (PDB code 1JFG); (b) *A. terreus* aristolochene synthase-Mg<sup>2+</sup><sub>3</sub>-PP<sub>i</sub> complex (PDB 2OA6); (c) *S. coelicolor* epi-isozizaene synthase-Mg<sup>2+</sup><sub>3</sub>-PP<sub>i</sub> complex (PDB code 3KB9); (d) *N. tabacum* 5-epi-aristolochene synthase-Mg<sup>2+</sup><sub>3</sub>-farnesyl hydroxyphosphonate complex (PDB code 5EAT; note that many of the metal-phosphate interactions indicated are too long to be considered inner-sphere metal coordination interactions); (e) *S. officinalis* (+)-bornyl diphosphate synthase-Mg<sup>2+</sup><sub>3</sub>-PP<sub>i</sub> complex (PDB code 1N22; metal ions are labeled according to the convention first established for trichodiene synthase); (f) *M. spicata* limonene synthase-Mn<sup>2+</sup><sub>3</sub>-FLPP complex (PDB code 2ONG; conserved hydrogen bonding is indicated between D353 and R315 despite poor geometry).

Superposition of unliganded and  $\text{Mg}^{2+}_3\text{-PP}_i$  complexed trichodiene synthase structures reveals conformational changes that cap the active site upon ligand binding. Overall, the rms deviation between the native and liganded structures is 1.4 Å for 349 C $\alpha$  atoms. Interestingly, upon ligand binding, D101 in the aspartate-rich motif forms a salt bridge with R304, which donates a hydrogen bond to  $\text{PP}_i$ . In addition to  $\text{Mg}^{2+}$  coordination interactions, the  $\text{PP}_i$  anion also accepts hydrogen bonds from R182, K232, and Y305. The D101-R304- $\text{PP}_i$  hydrogen bond network appears to link substrate binding with the transition between the open and closed active site conformations. Assuming that the diphosphate group of FPP triggers the same structural changes as observed for  $\text{PP}_i$ , the substrate is sequestered from bulk solvent and the complete trinuclear magnesium cluster triggers departure of the diphosphate leaving group to generate the carbocation that initiates the cyclization cascade. The seemingly conservative D100E mutation results in a 22-fold loss in catalytic activity (measured by  $k_{\text{cat}}/K_M$ ) and structural studies indicate that the additional methylene group of E100 perturbs the  $\text{Mg}^{2+}_3\text{-PP}_i$  complex such that  $\text{Mg}^{2+}_A$  binding is weakened, E233 breaks its coordination interaction with  $\text{Mg}^{2+}_B$ , and  $\text{Mg}^{2+}_C$  is dissociated; additionally, hydrogen bond interactions between  $\text{PP}_i$  and R182 and R304 are broken [36,37].

The role of the D101-R304 salt bridge in closing the trichodiene synthase active site has been explored in mutagenesis studies. The D101E mutation results in a moderate 5-fold decrease in catalytic activity; however, there are no crystal structures of this mutant available for study [38]. In contrast, the R304K mutant results in a 5000-fold decrease in catalytic activity, and the crystal structure of R304K trichodiene synthase complexed with  $\text{Mg}^{2+}_3\text{-PP}_i$ -(*R*)-azabisabolene reveals the loss of the expected hydrogen bond between K304 and D101 [39]. Although the  $\text{PP}_i$  binding motif remains intact in the R304K mutant, it is evident that the R304-D101 hydrogen bond is critical for properly activating the substrate diphosphate group. In contrast, while Y305 donates a hydrogen bond to  $\text{PP}_i$  in the wild-type enzyme complex with  $\text{Mg}^{2+}_3\text{-PP}_i$ , catalytic activity and  $\text{PP}_i$  binding are not significantly affected in the Y305F mutant [37,40].

Another fungal cyclase that has been the subject of extensive structural and functional study is aristolochene synthase, which is a sesquiterpene cyclase that catalyzes the cyclization of FPP to form (+)-aristolochene. Structures of aristolochene synthases from *Penicillium roqueforti* [41] and *Aspergillus terreus* [42] have been solved; these enzymes are related by 61 % amino acid sequence identity. Although there is no crystal structure of *P. roqueforti* aristolochene synthase complexed with  $\text{Mg}^{2+}_3\text{-PP}_i$ , the structure of the *A. terreus* aristolochene synthase  $\text{Mg}^{2+}_3\text{-PP}_i$  complex [42] (Fig. 4b) indicates conservation of the  $\text{Mg}^{2+}_3\text{-PP}_i$  binding motif first observed in trichodiene synthase [20].

The aspartate-rich motif of aristolochene synthase on helix D appears as **D<sup>90</sup>DXXE**. The carboxylate side chain of D90 coordinates to  $\text{Mg}^{2+}_A$  and  $\text{Mg}^{2+}_B$  with *syn,syn*-bidentate geometry, and is the only residue in the aspartate motif that coordinates to the  $\text{Mg}^{2+}$  ions. The carboxylate group of D91 makes a salt bridge with R304, and the final carboxylate in the motif is E119, which accepts a hydrogen bond from a water molecule coordinated to  $\text{Mg}^{2+}_A$ . The second metal-binding motif **N<sup>219</sup>DIYS<sup>223</sup>YEKE<sup>227</sup>** is located on helix H and chelates  $\text{Mg}^{2+}_B$  [42], consistent with the structures of terpenoid cyclases from plants, bacteria, and fungi [20,21,43–45]. As found in the active sites of trichodiene synthase [20] and epi-isozizaene synthase [43],  $\text{PP}_i$  binding in aristolochene synthase is similarly accommodated by hydrogen bonds donated from two arginines (R175 and F314), one lysine (K226), and one tyrosine (Y315) (Fig. 4b).

## Bacterial cyclases

In recent years, prokaryotes have emerged as sources of diverse isoprenoids. Specifically, a large number of novel isoprenoids have been isolated from organisms belonging to the taxonomical order *Actinomycetales* [46]. The crystal structures of two bacterial sesquiterpene cyclases have been solved, and both derive from *Actinomycetales*: pentalenene synthase from *Streptomyces* UC5319 [47] and epi-isozizaene synthase from *Streptomyces coelicolor* [43,48]. Pentalenene synthase catalyzes the cycliza-

tion of FPP to form the tricyclic sesquiterpene pentalenene in the first committed step in the biosynthesis of the pentalenolactone family of antibiotics [49]. Although the structure of pentalenene synthase was the first to be reported of a terpenoid cyclase and demonstrated that the terpenoid cyclase shared the FPP synthase fold first observed for avian FPP synthase [17], no structure of this bacterial terpenoid cyclase complexed with metal ions is available.

However, the crystal structure of epi-isozizaene synthase complexed with  $\text{Mg}^{2+}_3\text{-PP}_i\text{-BTAC}$  (BTAC is the benzyltriethylammonium cation, a crystallization additive) reveals that  $\text{Mg}^{2+}_3\text{-PP}_i$  binding motifs are conserved between fungal and bacterial terpenoid cyclases (Fig. 4c) [43]. The first aspartate of the aspartate-rich motif  $\text{D}^{99}\text{DRHD}$  coordinates to  $\text{Mg}^{2+}_A$  and  $\text{Mg}^{2+}_C$  with *syn,syn*-bidentate geometry, and  $\text{Mg}^{2+}_B$  is chelated by  $\text{N}^{240}\text{DLCS}^{244}\text{LPKE}^{248}$ . Each  $\text{Mg}^{2+}$  ion is coordinated with octahedral geometry and nonprotein coordination sites are occupied by oxygen atoms of  $\text{PP}_i$  and water molecules. The  $\text{PP}_i$  anion also accepts hydrogen bonds from the side chains of R194, K247, R338, and Y339 [43], which correspond to R182, K232, R304, and Y305 of trichodiene synthase [20] and R175, K226, R314, and Y315 of aristolochene synthase [42]. Pentalenene synthase and epi-isozizaene synthase share 24 % amino acid sequence identity, and residues that interact with  $\text{Mg}^{2+}$  ions or  $\text{PP}_i$  in epi-isozizaene synthase are conserved in pentalenene synthase. Superposition of the liganded closed structure of epi-isozizaene synthase with unliganded pentalenene synthase reveals a very similar alignment of the metal-binding motifs, with pentalenene synthase helices D and H 1.5 Å further apart than in epi-isozizaene. Accordingly, upon substrate or  $\text{PP}_i$  binding the active site of pentalenene synthase presumably undergoes a conformational change to a closed conformation comparable to that observed for the epi-isozizaene synthase  $\text{Mg}^{2+}_3\text{-PP}_i\text{-BTAC}$  complex.

Although the second aspartate of the epi-isozizaene synthase aspartate-rich motif, D100, does not directly interact with the  $\text{Mg}^{2+}$  ions or  $\text{PP}_i$ , it does accept a hydrogen bond from R338, which also donates a hydrogen bond to  $\text{PP}_i$  [43]. Site-directed mutagenesis reveals that the D100N mutation causes a >95 % loss of activity with respect to the native enzyme [50], suggesting that the D100N mutation disrupts the D100-R338- $\text{PP}_i$  hydrogen bond network presumed to be important for substrate recognition. As previously discussed, the second aspartate in the aspartate-rich motifs of trichodiene synthase and aristolochene synthase similarly stabilizes a hydrogen bond network with R304 and  $\text{PP}_i$  [20,42], so it appears that the bacterial and fungal cyclases share the same molecular strategy for linking the molecular recognition of the substrate diphosphate group with the active site closure mechanism.

The third aspartate in the aspartate-rich motif of epi-isozizaene synthase, D103, points away from the active site and makes no hydrogen bond interactions that are involved in substrate binding, as also observed in  $\text{Mg}^{2+}_3\text{-PP}_i$  complexes of trichodiene synthase. The absence of a structural or catalytic role for the terminal aspartate in the aspartate-rich motif of bacterial terpenoid cyclases is supported by mutagenesis of the corresponding residue in pentalenene synthase: the D84E mutation results in a mere 3-fold loss of catalytic activity (as measured by  $k_{\text{cat}}/K_M$ ), whereas the D80E and D81E mutations yield 3500- and 400-fold reductions in activity, respectively [51].

## Plant cyclases

5-Epi-aristolochene synthase from *Nicotiana tabacum* catalyzes the cyclization of FPP to form 5-epi-aristolochene in the first committed step in the biosynthesis of the antifungal phytoalexin capsidiol [44]. The first crystal structure determined of a plant terpenoid cyclase and the second terpenoid cyclase structure to be reported, the structure of 5-epi-aristolochene synthase reveals the presence of two domains [44]: a catalytically active C-terminal domain that adopts the  $\alpha$ -helical class I terpenoid synthase fold, and an N-terminal domain of unknown function that nevertheless exhibits an  $\alpha$ -helical fold similar to that of a class II terpenoid synthase [9]. Two metal-binding motifs are identified: an aspartate-rich motif  $\text{D}^{301}\text{DXXD}^{305}$ , and a  $\text{D}^{444}\text{DTAT}^{448}\text{YEVE}^{452}$  motif. While the binding of a trinuclear magnesium cluster was identified in the 5-epi-aristolochene synthase farnesyl hydroxyphosphonate complex (Fig. 4d), analysis of the structure reveals that many of the coordination interactions with  $\text{Mg}^{2+}$  ions

range 2.2–3.7 Å, longer than expected for ideal  $Mg^{2+}$  coordination [52]. This could suggest that the structure is that of a partially closed conformation. Nonetheless, D301 and D305 of the aspartate-rich motif coordinate to  $Mg^{2+}_A$  and  $Mg^{2+}_C$ , while the “DTE” motif chelates  $Mg^{2+}_B$ .

Interestingly, metal-binding motifs are shared between sesquiterpene cyclases and monoterpene cyclases from plants. The monoterpene cyclase (+)-bornyl diphosphate synthase catalyzes the cyclization of GPP to form (+)-bornyl diphosphate. This cyclization is unusual in that the substrate diphosphate group is reincorporated into the product. The structure of (+)-bornyl diphosphate synthase from *Salvia officinalis* was the first of a monoterpene cyclase [21], and remains the only monoterpene cyclase for which structures have been solved in unliganded and liganded states. The crystal structure of (+)-bornyl diphosphate synthase reveals the two-domain  $\alpha$ -helical architecture first observed for the plant sesquiterpene synthase 5-epi-aristolochene synthase: a catalytically active C-terminal domain adopting the class I terpenoid synthase fold, and an N-terminal domain adopting the class II terpenoid synthase fold (however, the N-terminal polypeptide caps the active site of the C-terminal domain in ligand complexes) [21]. The (+)-bornyl diphosphate synthase- $Mg^{2+}_3$ - $PP_i$  complex reveals that conserved metal-binding motifs and the  $PP_i$  anion (or the diphosphate group of the product itself, (+)-bornyl diphosphate) coordinate to 3  $Mg^{2+}$  ions (Fig. 4e). The first carboxylate of the **D<sup>351</sup>DXXD<sup>355</sup>** motif coordinates to  $Mg^{2+}_A$  and  $Mg^{2+}_C$  with *syn,syn*-bidentate geometry, and D355 bridges  $Mg^{2+}_A$  and  $Mg^{2+}_C$  with *syn,anti*-coordination stereochemistry. Interestingly, unlike metal binding in the active sites of bacterial and fungal cyclases, both the first and third aspartates in the DDXXD motif of plant terpenoid cyclases coordinate to the catalytic metal ions. The second metal-binding motif, **D<sup>496</sup>DKGT<sup>500</sup>SYFE<sup>504</sup>**, chelates  $Mg^{2+}_B$  [21]. In addition to metal ion coordination interactions, the  $PP_i$  anion accepts hydrogen bonds from R314, R493, and K512. Comparison of the structures of unliganded and  $Mg^{2+}_3$ - $PP_i$  complexed (+)-bornyl diphosphate synthase reveals several  $Mg^{2+}_3$ - $PP_i$  induced conformational changes; however, the rms deviation of 306 C $\alpha$  atoms in the catalytic C-terminal domain is only 0.6 Å [21], significantly lower than observed for ligand-induced conformational changes in trichodiene synthase (1.4 Å) [20] and aristolochene synthase (1.8 Å) [42].

The recent structure determination of another plant monoterpene cyclase, limonene synthase from *Mentha spicata* [45], similarly reveals conservation of a trinuclear metal cluster in a cyclization reaction that generates 94 % (–)-(4S)-limonene, and ~2 % myrcene, (–)- $\alpha$ -pinene, and (–)- $\beta$ -pinene [53]. Limonene synthase shares the 2-domain  $\alpha$ -helical fold common to plant terpenoid cyclases. Limonene synthase displays similar activity with  $Mg^{2+}$  or  $Mn^{2+}$  (a common feature of some terpenoid cyclases), and the structure of the enzyme has been determined in complex with 3  $Mn^{2+}$  ions and the intermediate analog 2-fluorolinalyl diphosphate (FLPP) (Fig. 4f) [45]. Metal coordination interactions are similar to those observed in (+)-bornyl diphosphate synthase [21]. In limonene synthase, the first carboxylate of the **D<sup>352</sup>DXXD<sup>356</sup>** motif coordinates to  $Mn^{2+}_A$  and  $Mn^{2+}_C$  with *syn,syn*-bidentate geometry, and one oxygen atom of D356 bridges  $Mn^{2+}_A$  and  $Mn^{2+}_C$  with *syn,anti*-coordination stereochemistry. Two out of three residues in the second metal-binding motif, **D<sup>496</sup>DLGT<sup>500</sup>SVEE<sup>504</sup>**, chelate  $Mg^{2+}_B$ ; the position of the side chain of E504 is not indicated and is presumably disordered. Additionally, the  $\gamma$ -hydroxyl of T500 is 3.2 Å away from  $Mg^{2+}_B$ , which is too long to be considered an inner-sphere coordination interaction. The diphosphate group of the bound intermediate analog FLPP accepts hydrogen bonds from R315, R493, and K512 [45].

Finally, the sesquiterpene cyclase (+)- $\delta$ -cadinene synthase from *Gossypium arboreum* (tree cotton) catalyzes the first committed step in the biosynthesis of the triterpene phytoalexin gossypol, a major defense metabolite synthesized by cotton plants [54]. The recently determined structure of the unliganded enzyme and its complex with 2-fluorofarnesyl diphosphate (2F-FPP) reveals that minimal structural deviations result from ligand binding (the rms deviations are 0.28 and 0.50 Å between unliganded and liganded monomers A (514 C $\alpha$  atoms) and B (494 C $\alpha$  atoms), respectively) [55]. In contrast with the plant terpenoid cyclases previously discussed [21,44,45], (+)- $\delta$ -cadinene synthase contains a second aspartate-rich motif in place of the DTE motif on helix H. As previously discussed, this

motif on helix H is common to chain elongation enzymes such as FPP synthase, and (+)- $\delta$ -cadinene synthase is unique among known class I terpenoid cyclases in that it contains two aspartate-rich motifs for metal coordination. The structure of the liganded enzyme reveals a putative  $\text{Mg}^{2+}_3$  cluster (weak electron density characterizes the three  $\text{Mg}^{2+}$  ions);  $\text{Mg}^{2+}_A$  and  $\text{Mg}^{2+}_C$  are coordinated by D307 and D311 of the first  $\text{D}^{307}\text{DXXD}^{311}$  motif, and  $\text{Mg}^{2+}_B$  is coordinated by D451 and E455 of the second aspartate-rich motif,  $\text{D}^{451}\text{DVAE}^{455}$  (Fig. 5). However, many of the carboxylate- $\text{Mg}^{2+}$  distances observed are too long for inner-sphere metal coordination interactions; therefore, the structure may reflect an incomplete transition between the “open” and “closed” active site conformations. The diphosphate moiety of 2F-FPP accepts one hydrogen bond from a nearby basic residue, R448.

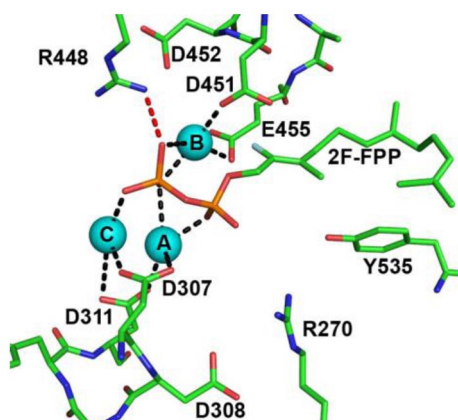


**Fig. 5** The diphosphate binding site of (+)- $\delta$ -cadinene synthase from *G. arboreum* (PDB code 3G4F) with a putative  $\text{Mg}^{2+}_3$  cluster and 2F-FPP bound. Metal ions are labeled according to convention established for trichodiene synthase. Some metal-phosphate interactions are too long to be considered inner-sphere coordination interactions, which could be a consequence of the nonproductive binding mode observed for 2F-FPP.

## DISCUSSION

Although the metal-dependence of catalysis by class I terpenoid synthases has been known for decades [56], it was not until 2001 that the crystal structure of a terpenoid cyclase- $\text{Mg}^{2+}_3$ - $\text{PP}_i$  complex (trichodiene synthase) revealed that a trinuclear metal cluster accommodates  $\text{PP}_i$  binding; this trinuclear metal cluster is similarly implicated in binding and activating substrate FPP for catalysis [20]. Since then, many X-ray crystal structures of isoprenoid coupling enzymes and terpenoid cyclases have been determined containing  $\text{Mg}^{2+}_3$  (or  $\text{Mn}^{2+}_3$ ) clusters. Comparisons of these structures reveal significant conservation in the constellation of metal ions and the residues that coordinate to these metal ions (Figs. 3 and 4) despite generally insignificant amino acid sequence identity among these enzymes.

Trinuclear metal cluster coordination in FPP synthases is conserved among humans, bacteria, and protozoans. Two aspartate-rich DDXXD binding motifs coordinate to 3  $\text{Mg}^{2+}$  ions, which are also coordinated by the substrate diphosphate group. The first and last aspartate in the first DDXXD motif coordinate to  $\text{Mg}^{2+}_A$  and  $\text{Mg}^{2+}_C$ , and the first aspartate of the second DDXXD motif coordinates to  $\text{Mg}^{2+}_B$ . Additionally conserved are one arginine and two lysine residues that donate hydrogen bonds to diphosphate oxygens; the conserved arginine residue also donates hydrogen bond(s) to the second aspartate in the first DDXXD motif (Figs. 3a–d). The crystal structures of other isoprenoid coupling enzymes, GGPP synthase and nonspecific prenyl synthase, similarly reveal conservation of  $\text{Mg}^{2+}_3$  binding motifs. Hydrogen bond interactions with  $\text{PP}_i$  are also conserved (Figs. 3e,f).

It is notable that the constellation of three metal ions and hydrogen bond donors is also conserved, with minor variations, in terpenoid cyclases from plants, bacteria, and fungi (Figs. 3a–f). First,  $Mg^{2+}_A$  and  $Mg^{2+}_C$  are coordinated by the first DDXXD motif: bacterial and fungal cyclases utilize only the first aspartate of this motif, whereas plant cyclases utilize the first and third aspartates of this motif (analogous to isoprenoid coupling enzymes). Second, the second aspartate-rich motif is usually replaced by an NDXXSXXXE motif in bacterial and fungal terpenoid cyclases and a DXXXTXXXE motif in plant terpenoid cyclases, in which boldface residues chelate  $Mg^{2+}_B$  (although there can be some variations in this sequence, e.g., see [57]). One exception, however, is (+)- $\delta$ -cadinenene synthase, in which two aspartate-rich motifs coordinate to the trinuclear metal cluster. Third, residues that donate hydrogen bonds to  $PP_i$  are conserved in terpenoid cyclases across different domains of life. Specifically, two arginines donate hydrogen bonds to diphosphate oxygens: one appears to replace a conserved lysine serving this function in the isoprenoid coupling enzymes, and the other also donates a hydrogen bond to the second aspartate of the first DDXXD motif (as observed in the isoprenoid coupling enzymes). In bacterial and fungal terpenoid cyclases, conserved lysine and tyrosine residues additionally donate hydrogen bonds to  $PP_i$ .

In all cases in which a complete  $Mg^{2+}_3-PP_i$  cluster is bound, two 6-membered ring chelates are formed with  $Mg^{2+}_A$  and  $Mg^{2+}_B$  (Fig. 6). The conformations of these 6-membered rings can vary, e.g., sofa, half-chair, etc. Such 6-membered ring chelates are occasionally observed in metal-diphosphate binding interactions, e.g., in the binding of the substrate analog imidodiphosphate to inorganic pyrophosphatase [58]. Although the class I terpenoid synthase fold and metal-pyrophosphate binding motif are conserved among isoprenoid coupling enzymes and terpenoid cyclases, it is interesting that the substrate orientation with regard to the trinuclear metal cluster appears to be opposite in these two groups of enzymes that have yielded structures to date: that is, the terminal phosphate group of an isoprenoid diphosphate group does not coordinate to  $Mg^{2+}_C$  in an isoprenoid coupling enzyme (Fig. 3e), but it does in a terpenoid cyclase (Fig. 4f).

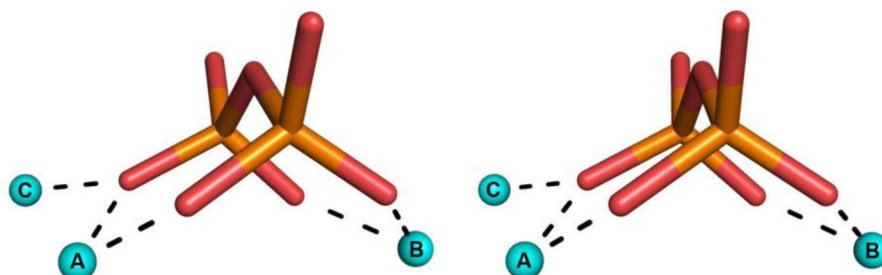


**Fig. 6** Stereoview of the  $Mg^{2+}_3-PP_i$  cluster from epi-isozizaene synthase [43]. Dashed lines (black) represent metal coordination interactions. The  $PP_i$  anion forms 6-membered ring chelates with  $Mg^{2+}_A$  and  $Mg^{2+}_B$ , both of which adopt distorted sofa conformations.

In summary, conservation of a trinuclear metal cluster is critical for catalysis by class I terpenoid synthases. This cluster not only serves to bind and orient the flexible isoprenoid substrate in the pre-catalytic Michaelis complex, but it also triggers leaving group departure and initial carbocation formation. Conserved hydrogen bond donors in the terpenoid synthase active site assist the metal cluster in this function. That the trinuclear metal cluster is conserved for catalysis by terpenoid synthases from many domains of life suggests a common ancestry for this family of enzymes in the evolution of terpenoid biosynthesis.

## ACKNOWLEDGMENTS

This work was supported by an NIH Chemical Biology Interface training grant (to J.A.A.) and NIH Grant GM56838 (to D.W.C.).

## REFERENCES

1. D. W. Christianson. *Science* **316**, 60 (2007).
2. A. Aharoni, M. A. Jongsma, H. J. Bouwmeester. *Trends Plant Sci.* **10**, 594 (2005).
3. E. Pichersky, J. P. Noel, N. Dudareva. *Science* **311**, 808 (2006).
4. J.-M. Rondeau, F. Bitsch, E. Bourgier, M. Geiser, R. Hemmig, M. Kroemer, S. Lehmann, P. Ramage, S. Rieffel, A. Strauss, J. R. Green, W. Jahnke. *ChemMedChem* **1**, 267 (2006).
5. A. G. Agrawal, R. R. Somani. *Mini Rev. Med. Chem.* **9**, 638 (2009).
6. A. A. Licata. *Ann. Pharmacother.* **39**, 668 (2005).
7. F. H. Ebetino, C. N. Roze, C. E. McKenna, B. L. Barnett, J. E. Dunford, R. G. G. Russell, G. E. Mieling, M. J. Rogers. *J. Organomet. Chem.* **690**, 2679 (2005).
8. H. V. Thulasiram, H. K. Erickson, C. D. Poulter. *Science* **316**, 73 (2007).
9. K. U. Wendt, G. E. Schulz. *Structure* **6**, 127 (1998).
10. C. A. Lesburg, J. M. Caruthers, C. M. Paschall, D. W. Christianson. *Curr. Opin. Struct. Biol.* **8**, 695 (1998).
11. R. Croteau, D. E. Cane. *Methods Enzymol.* **110**, 383 (1985).
12. D. E. Cane. *Chem. Rev.* **90**, 1089 (1990).
13. Y. Yoshikuni, T. E. Ferrin, J. D. Keasling. *Nature* **440**, 1078 (2006).
14. M. B. Austin, P. E. O'Maille, J. P. Noel. *Nat. Chem. Biol.* **4**, 217 (2008).
15. D. W. Christianson. *Chem. Rev.* **106**, 3412 (2006).
16. D. W. Christianson. *Curr. Opin. Chem. Biol.* **12**, 141 (2008).
17. L. C. Tarshis, M. Yan, C. D. Poulter, J. C. Sacchettini. *Biochemistry* **33**, 10871 (1994).
18. M. N. Ashby, P. A. Edwards. *J. Biol. Chem.* **265**, 13157 (1990).
19. D. J. Hosfield, Y. Zhang, D. R. Dougan, A. Broun, L. W. Tari, R. V. Swanson, J. Finn. *J. Biol. Chem.* **279**, 8526 (2004).
20. M. J. Rynkiewicz, D. E. Cane, D. W. Christianson. *Proc. Natl. Acad. Sci. USA* **98**, 13543 (2001).
21. D. A. Whittington, M. L. Wise, M. Urbansky, R. M. Coates, R. B. Croteau, D. W. Christianson. *Proc. Natl. Acad. Sci. USA* **99**, 15375 (2002).
22. H. B. Tanowitz, F. S. Machado, L. A. Jelicks, J. Shirani, A. C. de Carvalho, D. C. Spray, S. M. Factor, L. V. Kirchoff, L. M. Weiss. *Prog. Cardiovasc. Dis.* **51**, 524 (2009).
23. L. R. Garzoni, A. Caldera, M. d. N. Meirelles, S. L. de Castro, R. Docampo, G. A. Meints, E. Oldfield, J. A. Urbina. *Int. J. Antimicrob. Agents* **23**, 273 (2004).
24. S. B. Gabelli, J. S. McLellan, A. Montalvetti, E. Oldfield, R. Docampo, L. M. Amzel. *Proteins: Struct. Funct. Bioinf.* **62**, 80 (2006).
25. Y. Zhang, R. Cao, F. Yin, M. P. Hudock, R.-T. Guo, K. Krysiak, S. Mukherjee, Y.-G. Gao, H. Robinson, Y. Song, J. H. No, K. Bergan, A. Leon, L. Cass, A. Goddard, T.-K. Chang, F.-Y. Lin, E. Van Beek, S. Papapoulos, A. H. Wang, T. Kubo, M. Ochi, D. Mukkamala, E. Oldfield. *J. Am. Chem. Soc.* **131**, 5153 (2009).
26. J. Mao, S. Mukherjee, Y. Zhang, R. Cao, J. M. Sanders, Y. Song, Y. Zhang, G. A. Meints, Y. G. Gao, D. Mukkamala, M. P. Hudock, E. Oldfield. *J. Am. Chem. Soc.* **128**, 14485 (2006).
27. R. G. G. Russell. *Ann. N.Y. Acad. Sci.* **1068**, 367 (2006).
28. K. Nishio, Y. Nodake, K. Hamada, K. Suto, N. Nakagawa, S. Kuramitsu, K. Miura. *Acta Crystallogr., Sect. D: Biol. Crystallogr.* **60**, 178 (2004).
29. D. P. Kloer, R. Welsch, P. Beyer, G. E. Schulz. *Biochemistry* **45**, 15197 (2006).
30. T.-H. Chang, R.-T. Guo, T.-P. Ko, A. H.-J. Wang, P.-H. Liang. *J. Biol. Chem.* **281**, 14991 (2006).

31. K. L. Kavanagh, J. E. Dunford, G. Bunkoczi, R. G. G. Russell, U. Oppermann. *J. Biol. Chem.* **281**, 22004 (2006).
32. C. K.-M. Chen, M. P. Hudock, Y. Zhang, R.-T. Guo, R. Cao, J. H. No, P.-H. Liang, T.-P. Ko, T.-H. Chang, S.-C. Chang, Y. Song, J. Axelson, A. Kumar, A. H. Wang, E. Oldfield. *J. Med. Chem.* **51**, 5594 (2008).
33. J. D. Artz, J. E. Dunford, M. J. Arrowood, A. Dong, M. Chruszcz, K. L. Kavanagh, W. Minor, R. G. G. Russell, F. H. Ebetino, U. Oppermann, R. Hui. *Chem. Biol.* **15**, 1296 (2008).
34. S. A. Hashsham, L. M. Wick, J.-M. Rouillard, E. Gulari, J. M. Tiedje. *Biosens. Bioelectron.* **20**, 668 (2004).
35. Y. J. Hong, D. J. Tantillo. *J. Am. Chem. Soc.* **131**, 7999 (2009).
36. M. J. Rynkiewicz, D. E. Cane, D. W. Christianson. *Biochemistry* **41**, 1732 (2002).
37. L. S. Vedula, M. J. Rynkiewicz, H. J. Pyun, R. M. Coates, D. E. Cane, D. W. Christianson. *Biochemistry* **44**, 6153 (2005).
38. D. E. Cane, Q. Xue, B. C. Fitzsimons. *Biochemistry* **35**, 12369 (1996).
39. L. S. Vedula, D. E. Cane, D. W. Christianson. *Biochemistry* **44**, 12719 (2005).
40. D. E. Cane, J. H. Shim, Q. Xue, B. C. Fitzsimons, T. M. Hohn. *Biochemistry* **34**, 2480 (1995).
41. J. M. Caruthers, I. Kang, M. J. Rynkiewicz, D. E. Cane, D. W. Christianson. *J. Biol. Chem.* **275**, 25533 (2000).
42. E. Y. Shishova, L. Di Costanzo, D. E. Cane, D. W. Christianson. *Biochemistry* **46**, 1941 (2007).
43. J. A. Aaron, X. Lin, D. E. Cane, D. W. Christianson. *Biochemistry* **49**, 1787 (2010).
44. C. M. Starks, K. Back, J. Chappell, J. P. Noel. *Science* **277**, 1815 (1997).
45. D. C. Hyatt, B. Youn, Y. Zhao, B. Santhamma, R. M. Coates, R. B. Croteau, C. Kang. *Proc. Natl. Acad. Sci. SA* **104**, 5360 (2007).
46. M. Daum, S. Herrmann, B. Wilkinson, A. Bechthold. *Curr. Opin. Chem. Biol.* **13**, 180 (2009).
47. C. A. Lesburg, G. Zhai, D. E. Cane, D. W. Christianson. *Science* **277**, 1820 (1997).
48. X. Lin, R. Hopson, D. E. Cane. *J. Am. Chem. Soc.* **128**, 6022 (2006).
49. H. Seto, H. Yonehara. *J. Antibiot. (Tokyo)* **33**, 92 (1980).
50. X. Lin, D. E. Cane. *J. Am. Chem. Soc.* **131**, 6332 (2009).
51. M. Seemann, G. Zhai, J.-W. de Kraker, C. M. Paschall, D. W. Christianson, D. E. Cane. *J. Am. Chem. Soc.* **124**, 7681 (2002).
52. H. Zheng, M. Chruszcz, P. Lasota, L. Lebioda, W. Minor. *J. Inorg. Biochem.* **102**, 1765 (2008).
53. D. C. Williams, D. J. McGarvey, E. J. Katahira, R. Croteau. *Biochemistry* **37**, 12213 (1998).
54. X.-Y. Chen, Y. Chen, P. Heinsteins, V. J. Davisson. *Arch. Biochem. Biophys.* **324**, 255 (1995).
55. H. A. Gennadios, V. Gonzalez, L. Di Costanzo, A. Li, F. Yu, D. J. Miller, R. K. Allemann, D. W. Christianson. *Biochemistry* **48**, 6175 (2009).
56. D. R. Robinson, C. A. West. *Biochemistry* **9**, 70 (1970).
57. K. Zhou, R. J. Peters. *Phytochemistry* **70**, 366 (2009).
58. I. P. Fabrichniy, L. Lehtio, M. Tammenkoski, A. B. Zyryanov, E. Oksanen, A. A. Baykov, R. Lahti, A. Goldman. *J. Biol. Chem.* **282**, 1422 (2007).